JVST B
Journal of Vacuum Science & Technology B

ARTICLE

pubs.aip.org/avs/jvb

Development of GeSn epitaxial films with strong direct bandgap luminescence in the mid-wave infrared region using a commercial chemical vapor deposition reactor

Cite as: J. Vac. Sci. Technol. B **42**, 052210 (2024); doi: 10.1116/6.0003798
Submitted: 31 May 2024 · Accepted: 15 August 2024 ·
Published Online: 17 September 2024

Nicholas Rosson,[1] Sudip Acharya,[2] Alec M. Fischer,[1] Bria Collier,[2] Abdulla Ali,[2] Ali Torabi,[1] Wei Du,[2,3] Shui-Qing Yu,[2,3] and Robin C. Scott[1,a)]

AFFILIATIONS

[1]Lawerence Semiconductor Research Laboratory, Inc., 2300 West Huntington Drive, Tempe, Arizona 85282
[2]Materials Science and Engineering, University of Arkansas, Fayetteville, Arkansas 72701
[3]Department of Electrical Engineering and Computer Science, University of Arkansas, Fayetteville, Arkansas 72710

Note: This paper is part of the 2024 Special Topic Collection on Developing SiGeSn Technology: Materials and Devices.
[a)]**Author to whom correspondence should be addressed:** rscott@lsrl.com

ABSTRACT

Germanium tin (GeSn) is a material of interest for electronic and photonic device applications, but its development and commercialization have been limited by material quality issues and lack of availability from epitaxy suppliers. In this paper, we report initial studies in optimizing GeSn films deposited on a Ge buffer layer grown on 200-mm diameter silicon (Si) substrates with an ASM Epsilon 2000 chemical vapor deposition reactor designed for commercial production. Using a single-step growth process, a Sn content up to 22% near the surface of a GeSn film was achieved due to the increase in Sn incorporation via strain relaxation. A two-step growth process resulted in a bilayer structure with a nearly 100% relaxation on the first layer, followed by a higher quality GeSn layer with 18% Sn as evident by a high photoluminescence intensity emitting in the mid-wave infrared region at 3.2 μm at 20 K.

I. INTRODUCTION

GeSn-based electronic and photonic devices have been gaining interest in the semiconductor device industry due to the direct bandgap behavior at Sn compositions above ~7% and potential for monolithic integration of GeSn device structures onto low-cost Si-based platforms. Traditionally, III-V and II-VI materials have been used for optoelectronic devices that rely on direct bandgap materials which are costly compared to group IV Si-based materials. Heterointegration of III-V materials with silicon has been extensively studied and has proven challenging[1] due to the differences in lattice parameter and coefficient of thermal expansion (CTE).[2,3] Other approaches such as thermo-compressive bonding have also been utilized,[4] but not adopted for large scale production. Device fabrication with compound semiconductor materials can have significant manufacturing challenges. For example, many of the precursors used in III-V and II-VI materials growth via metal-organic chemical vapor deposition (MOCVD) are toxic,[5] pyrophoric, and are subject to stringent waste effluent regulations requiring costly abatement systems. In addition, III-V and II-VI substrates needed for epitaxial growth are not always commercially available. As an alternative, researchers are studying GeSn and SiGeSn expecting to create a disruptive technological milestone.[6,7] The fundamental optoelectronic device limitation for traditional group IV semiconductor materials has been the indirect bandgap. However, by alloying Ge with Sn at Sn compositions greater than ~7%, GeSn becomes a direct bandgap semiconductor.[8–10] The GeSn bandgap can theoretically be tuned over a wide range extending from the short-wave to the long-wave infrared (SWIR-LWIR) regions of the electromagnetic spectrum, enabling the realization of group IV optoelectronics devices such as lasers, detectors, and

modulators monolithically integrated onto silicon substrates.[11–13] Given the reduction in effective mass when Sn is added to the Ge lattice, higher carrier mobilities are possible, expanding applications for GeSn to include logic and quantum devices.[11,14] Despite evidence that GeSn is theoretically viable for device applications, achieving high quality GeSn material quality is challenging due to the high lattice mismatch between Ge and Sn (~15%), the low solubility (<1%) of Sn in Ge, and the instability of α-Sn above 13 °C. To address these challenges, a variety of growth methods have been studied including molecular beam epitaxy (MBE),[15,16] chemical vapor deposition (CVD),[17,18] and remote plasma-enhanced chemical vapor deposition (RPECVD).[19] The CVD growth technique has been widely investigated to achieve high Sn incorporation for device performance expectations. As CVD-grown GeSn is deposited at relatively low temperatures, higher-order hydrides such as digermane which decompose at lower temperatures are preferred.[20,21] However, the lower cost of germane (GeH_4) and tin tetrachloride ($SnCl_4$), hydrogen and nitrogen carrier gases are more favorable for large scale manufacturing.[22]

In this study, we evaluate the surface morphology, Sn segregation, and composition and strain of GeSn films grown on 200-mm substrates by CVD when varying process parameters including hydrogen carrier gas flow rate, deposition temperature, $GeH_4/SnCl_4$ molar flow ratio, and $SnCl_4$ molar flow rate.

II. EXPERIMENT

An ASM Epsilon 2000 reduced-pressure CVD reactor was used to grow undoped GeSn films on a 1.2-μm-thick relaxed Ge buffer layer deposited on lightly B-doped 200-mm-diameter (001) silicon substrates. The growth of Ge and GeSn films was carried out using germane (GeH_4) diluted in a 10% hydrogen gas balance and tin tetrachloride ($SnCl_4$) precursors with hydrogen as the main carrier gas.

Prior to starting epitaxial growth, the silicon wafer was baked at 1100 °C to ensure the removal of the native oxide layer, exposing a pristine silicon surface. A dedicated liquid delivery system was installed for the $SnCl_4$ bubbler with a controlled temperature at 20 °C, providing a $SnCl_4$ vapor pressure of 24 mbar. The Ge buffer layer was deposited directly on the silicon substrate using a two-step approach: a low-temperature thin Ge seed layer followed by a high-temperature thick Ge bulk layer in order to reduce the threading dislocation density (TDD).[23] GeSn growth was carried out at temperatures ranging from 240 to 320 °C and at high pressures to reduce Sn segregation.[24] The molar flow ratio of precursors $SnCl_4/(SnCl_4 + GeH_4 + H_2)$ was varied from 10^{-6} to 10^{-5}. The GeSn layer thickness uniformity was measured along the wafer diameter using spectroscopic ellipsometry (SE, Woollam M2000). The GeSn surface morphology was evaluated using a collimated bright-light source (home-built), optical microscope images (Nikon Eclipse L200) at 200 and 1000× magnification, and atomic force microscopy (AFM, Bruker Dimension 3100). The threading dislocation density of the GeSn epilayer and Ge buffer layer was revealed using a modified Dash etch process and measured by AFM.[25] Secondary-ion mass spectrometry (SIMS, Atomika 4100) profiles were performed by Eurofins EAG Laboratories to quantify the Sn content in the GeSn film as a function of thickness. The approximated Sn content was calculated using Omega-2Theta x-ray diffraction (XRD, Rigaku SmartLab) scans, while the absolute Sn content and the degree of relaxation in the GeSn films were validated by reciprocal space maps (RSMs). The optical quality of GeSn films was characterized by room- (300 K) and low-temperature (20 K) photoluminescence (PL) spectroscopy using a 532 nm continuous-wave and a 1064 nm pulsed laser.

III. RESULTS AND DISCUSSION

A. Ge buffer layer

The surface morphology of the Ge buffer layer was evaluated by AFM. The as-deposited Ge surface is smooth and exhibits cross-hatch lines indicating that the film is fully relaxed, see Fig. 1(a). The average surface roughness R_a and the root-mean-square (RMS) roughness R_q are 0.491 and 0.615 nm, respectively. The threading dislocation density (TDD) in the Ge layer is about $4\ cm^{-2} \times 10^7/cm^2$, as shown in Fig. 1(b) post etch pit decoration.

B. GeSn process tuning

1. Segregation control

a. Hydrogen carrier gas flow rate. Initially, the influence of hydrogen carrier gas flow on surface morphology of the GeSn layer was studied at a relatively high CVD growth pressure, fixed deposition temperature of 320 °C, and with $SnCl_4$ and GeH_4 molar flow rates at 3.5×10^{-5} and 1.8×10^{-3} moles/min, respectively. At the higher hydrogen carrier flow rates, the GeSn surface morphology is poor with macroscopic Sn segregation (haze) across the entire wafer surface as shown in Figs. 2(a) and 2(b), whereas at the lower hydrogen flow rates the GeSn surface across the wafer is mostly specular, as shown in Figs. 2(c) and 2(d).

Though the GeSn films grown at high hydrogen flow rates have Sn segregation across the entire 200-mm surface, the amount of Sn segregation encroaching from the wafer edge to center is reduced by increasing the GeH_4 molar flow rate from 1.8×10^{-3} to 4.8×10^{-3} mol/min [compare Figs. 2(a) and 2(e)][26] or by increasing the deposition temperature [compare Figs. 2(b) and 2(f)]. We believe that more Sn segregation on the surface is observed at higher hydrogen carrier flow rates due to a decrease in the *effective* $GeH_4/SnCl_4$ or reactant product ratio at the surface even though the $SnCl_4$ and GeH_4 are "equivalently" diluted. In considering thermal dissociation of precursors, at the highest hydrogen carrier flow rate, i.e., highest gas flow velocity, there is a reduction in the residence time for the reactive gases flowing across the heated susceptor/wafer and consequently a reduction in the thermal decomposition of GeH_4 and/or $SnCl_4$. The GeH_4 pyrolysis is likely suppressed at higher hydrogen flow rates and $SnCl_4$ may be partially decomposed before arriving at the heated susceptor/wafer surface.[27] At the lowest hydrogen carrier flow rate, the growth rate is lower than that of the intermediate and higher hydrogen carrier flow rates with an apparent depletion of $SnCl_4$ from edge to center based on SE thickness measurements. The GeSn layer thickness is ~176 nm at the edge and 0 nm at the center of the wafer. The Omega-2Theta XRD scan in Fig. 3 of wafers in Fig. 2(d) reveals a GeSn peak at the edge of the wafer (black solid line) corresponding to a Sn content of ~2%, while no GeSn diffraction peak is observed at the center of the wafer (black dashed line).

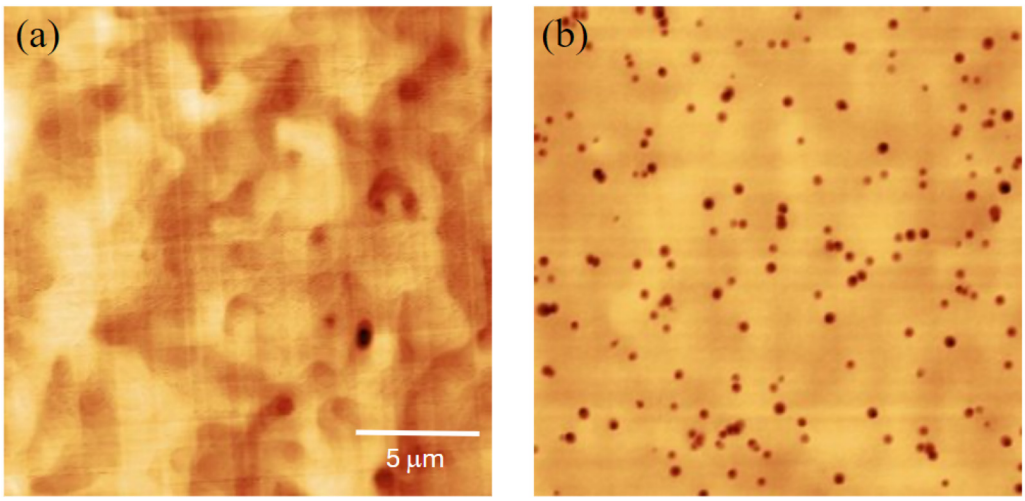

FIG. 1. 20 × 20 μm^2 AFM images of the Ge buffer layer (a) as-deposited and (b) after etch pit decoration.

We believe that there are two plausible explanations for the low growth rates (1.2–4.5 nm/min) and edge-to-center thickness depletion at the lowest hydrogen carrier gas flow rate. For one, the larger molecular weight of $SnCl_4$ compared to other group IV precursors such as GeH_4, coupled with a slow carrier gas velocity may result in complete consumption of dissociated $SnCl_4$ in growing GeSn at the edge of the wafer (gas inlet located near wafer edge) with no $SnCl_4$ remaining for GeSn growth at the center of the wafer. Second, the increased chlorine to hydrogen concentration at low hydrogen flow rates could promote etching versus deposition.

Finally, we found that an intermediate hydrogen carrier gas flow rate [see Fig. 2(c)] is optimum for high-quality GeSn films, exhibiting improved layer thickness and Sn composition uniformity (<2%) for Sn content up to 12%, while maintaining a specular surface across ~99% of the wafer and a ~0.5 cm Sn segregation ring near the edge of the wafer. For higher Sn compositions at 18–20%, there is a segregation ring of ~3.5 cm in from the edge of the wafer.

b. $SnCl_4$ molar flow rate. The effect of increasing $SnCl_4$ molar flow rate on the Sn surface segregation was evaluated using collimated bright-light and optical microscope images. The microscope images taken at the edge refer to an area at the outer most diameter where the wafer remains specular (no segregation). Figures 4(a)–4(c) correspond to GeSn films with Sn contents at the center of the wafers of 4.37,

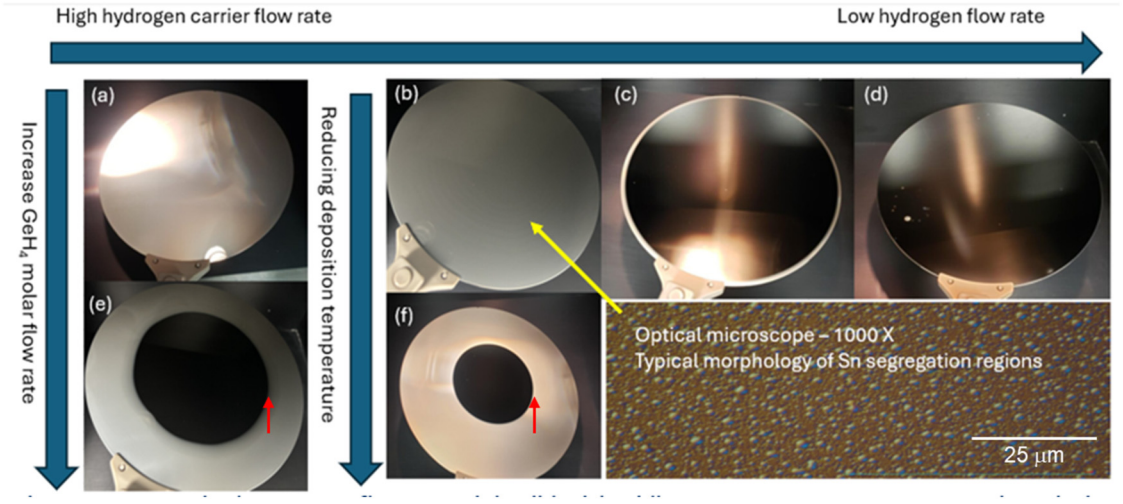

FIG. 2. Trends in Sn segregation [(a)–(d)] by lowering the hydrogen carrier gas flow rate, [(a) and (e)] by increasing the GeH_4 molar flow ratio, and [(b) and (f)] by reducing deposition temperature. Red arrows point to the edge of the Sn segregated region.

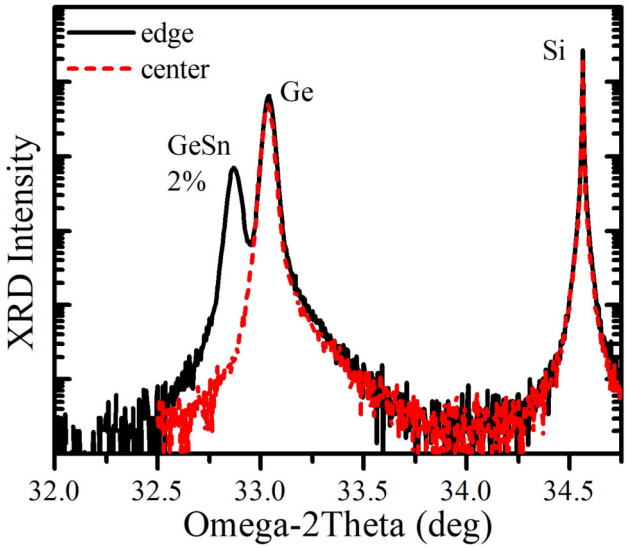

FIG. 3. Omega-2Theta XRD scans showing GeSn diffraction peaks (edge) near the wafer edge (black solid line) and (center) at the center of the wafer (black dashed line) from Fig. 2(d).

4.77, and 4.98% measured by XRD and grown using $SnCl_4$ molar flow rates of 3.6, 7.2, and 11×10^{-5} moles/min, respectively. Though the Sn concentration at the center of the wafer and the Sn segregation encroachment increase from the edge toward the center of the wafer with increasing $SnCl_4$ molar flow rates, the Sn concentration at the edge of the wafer decreases from 5.58% to 4.5% with increasing $SnCl_4$ molar flow rates, presumably due to the Sn contribution to segregation at the surface instead of Sn incorporating into the GeSn lattice.

c. Growth temperature. Previous studies have shown that the epitaxial growth of GeSn is only possible within a limited temperature range.[28–30] In this section, GeSn layers grown at temperatures ranging from 260 to 320 °C were investigated. The morphology, composition, and thickness of GeSn films are shown in Fig. 5. The area of segregated Sn seen at the surface edge of the wafers is similar for all samples, i.e., independent of growth temperature, suggesting that the Sn segregation is not temperature dependent over this temperature range and process space.

2. Dependence of growth temperature on growth rate and Sn incorporation

The effect of deposition temperature on the growth rate and Sn incorporation are shown in Fig. 6. Our study shows that the growth rate increases with the increasing growth temperature while the Sn incorporation decreases. The former can be explained by the increase in GeH_4 reactivity at elevated temperatures. The latter is a consequence of reduced Sn adatom mobility.[27–29]

3. Thickness uniformity

Most Si-based alloys grown in a CVD reactor at low temperatures (<600 °C) occur in the reaction rate-limited regime, where growth rate is dictated by temperature as shown on the Arrhenius

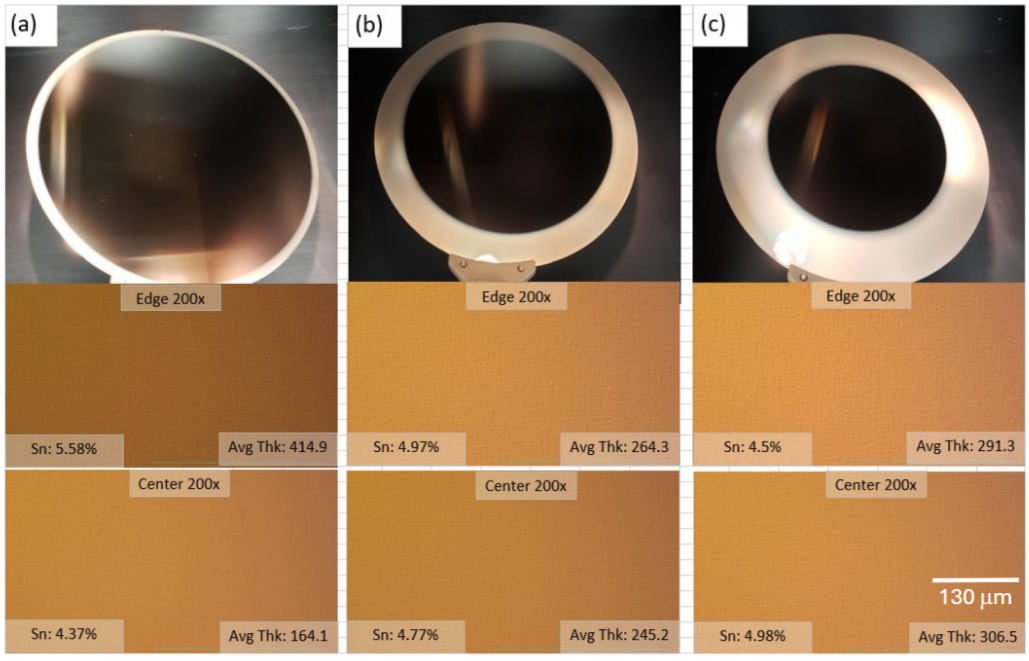

FIG. 4. Bright-light and optical images of GeSn films showing the dependence of $SnCl_4$ molar flow rates, (a) 3.6×10^{-5} moles/min, (b) 7.2×10^{-5} moles/min, and (c) 11×10^{-5} moles/min on Sn content and segregation encroachment.

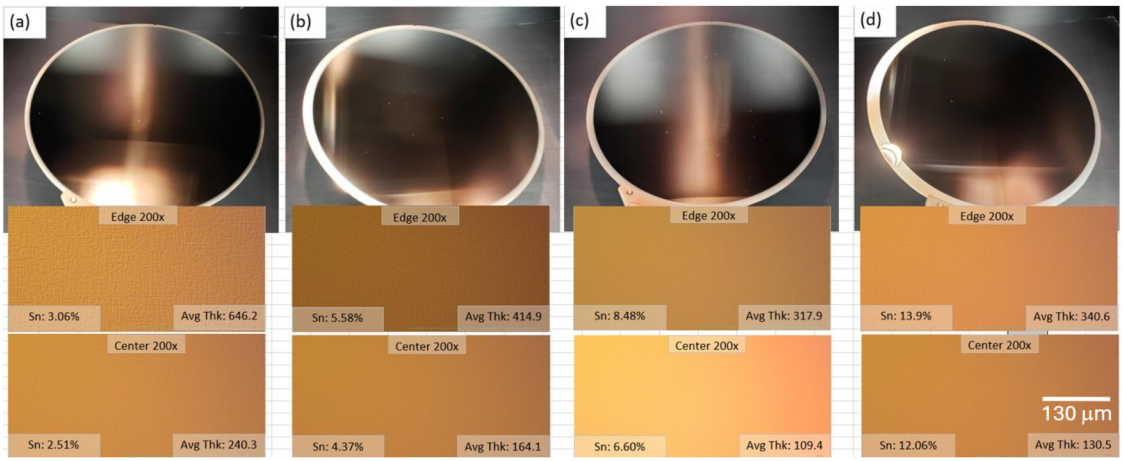

FIG. 5. Sn segregation, composition, thickness, and morphology at deposition temperatures of (a) 320 °C, (b) 300 °C, (c) 285 °C, and (d) 260 °C.

plot in Fig. 7. For Ge-based alloys grown using GeH_4, the mass transport regime dominates growth at deposition temperatures ranging from 400 to ~650 °C.

In our work, GeSn film thickness uniformity across the wafer diameter was studied as a function of (1) deposition temperature, by adjusting the temperature offsets relative to the center setpoint temperature, and (2) the gas flow distribution, by adjusting the relative orifice dimensions of the five-port gas injectors. Reducing the temperature offsets by 10 °C had minimal effect on the growth rate uniformity, as shown in Fig. 8(a) $T_{nominal}$ versus $T_{-10\,°C}$. The gas flow distribution was evaluated at a growth temperature of 260 °C, where the Sn composition is ~9% across the wafer. The redistribution of gases injected into the reactor reduces the growth rate nonuniformity across the wafer (*BA* more uniform than *AY* and *AU*) as shown in Fig. 8(b). This is consistent with the trend in Fig. 7 using a GeH_4 precursor, where epitaxial growth persists in the mass transport limited growth regime at low deposition temperatures.

C. Physical properties of GeSn

After optimizing critical growth parameters for the GeSn films, additional GeSn samples were grown with varied layer thickness and Sn composition to study their optical and structural properties. These samples were grown between 240 and 320 °C. The results from the center region of the wafers are shown in Table I.

1. Sn content

Sn concentration depth profiles of the GeSn layers were measured by SIMS as shown in Fig. 9. Samples *BJ*, *BO*, *BQ*, and *BR* were all grown using a single-step growth process consisting of a

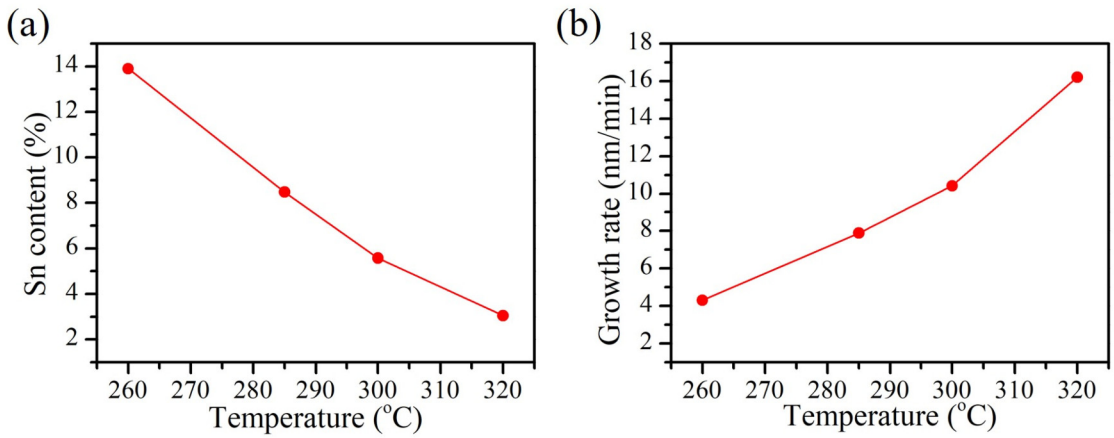

FIG. 6. (a) Sn incorporation and (b) growth rate as a function of growth temperature, measured by XRD and SE, respectively.

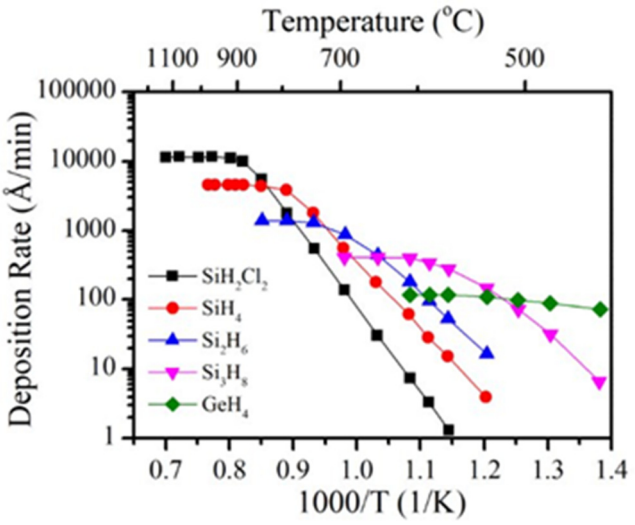

FIG. 7. Arrhenius plot of Si and Ge deposition rate for various precursors. Data taken from Ref. 31.

single deposition condition, where we see a continuous increase in Sn concentration of ~5%–8% with grown thickness, Figs. 9(a)–9(d), due to spontaneous strain relaxation of the GeSn at the growth interface.[32] However, when using a two-step growth process which consists of a high deposition temperature followed by a lower one ranging from 230 to 270 °C, as shown for sample *BP* in Fig. 9(e), the second layer reveals a constant Sn composition of ~17% with 70% film relaxation grown on a nearly fully relaxed first layer (see Table I). This first layer is responsible for the high Sn achieved in the second grown layer.[33,34] The abrupt increase in Sn composition at a depth of ~500 nm from the surface is where the growth interruption occurred.

2. Lattice strain

The degree of relaxation R of the GeSn films grown on the Ge buffer layer was measured from the (224) GeSn and (224) Ge diffraction spots by using the following equation:

$$R = \frac{a_{\mathrm{GeSn}}^{\mathrm{strained}} - a_{\mathrm{Ge}}}{a_{\mathrm{GeSn}}^{\mathrm{relaxed}} - a_{\mathrm{Ge}}},$$

where a_{Ge} is the lattice parameter of the Ge buffer (3%–4% tensile strained) and $a_{\mathrm{GeSn}}^{\mathrm{strained}}$ corresponds to the in-plane GeSn lattice

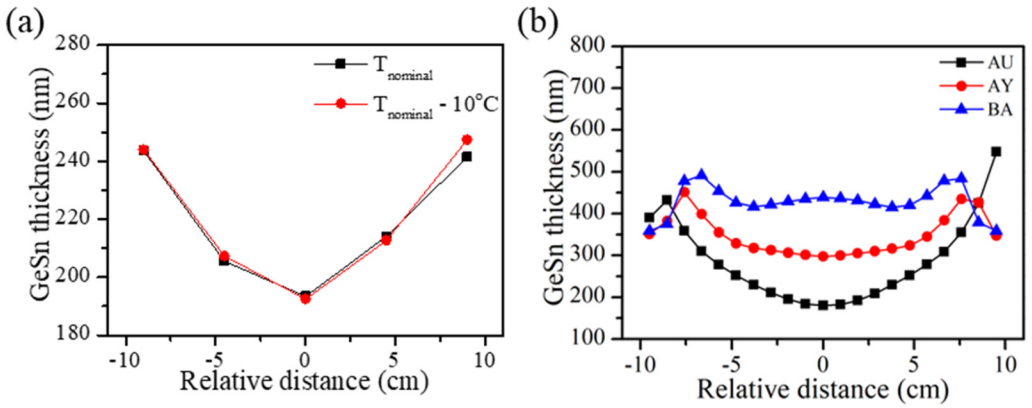

FIG. 8. GeSn thickness tuning across 200 mm wafers by (a) temperature offset and (b) five-port injector adjustments with optimum thickness uniformity in *BA*.

TABLE I. GeSn film thickness, surface roughness, Sn content, degree of relaxation, and threading dislocation density (TDD).

Sample	GeSn thickness (nm)	R_a (nm)	R_q (nm)	[Sn] (%)top/bottom[a]	Degree of relaxation (%)top/bottom[a]	TDD (10^7 cm^{-2})
AN	130	1.6	2.0	7.2/NA	6.0/NA	7.5
AR	243	3.6	4.5	8.5/7.6	64.0/67.0	3.5
BJ	470	6.0	7.4	15.7/12.8	56.0/67.2	6.0
BO	572	9.3	7.2	17.1/13.7	66.5/81.2	7.1
BP	836	10.9	9.2	16.9/10.3	74.0/92.0	7.5
BQ	533	8.8	10.5	17.5/13.7	67.2/81.2	9.9
BR	800	14.1	10.9	17.9/13.4	79.3/89.0	8.0

[a]Top/bottom refers to bulk regions within the GeSn films as measured by RSM.

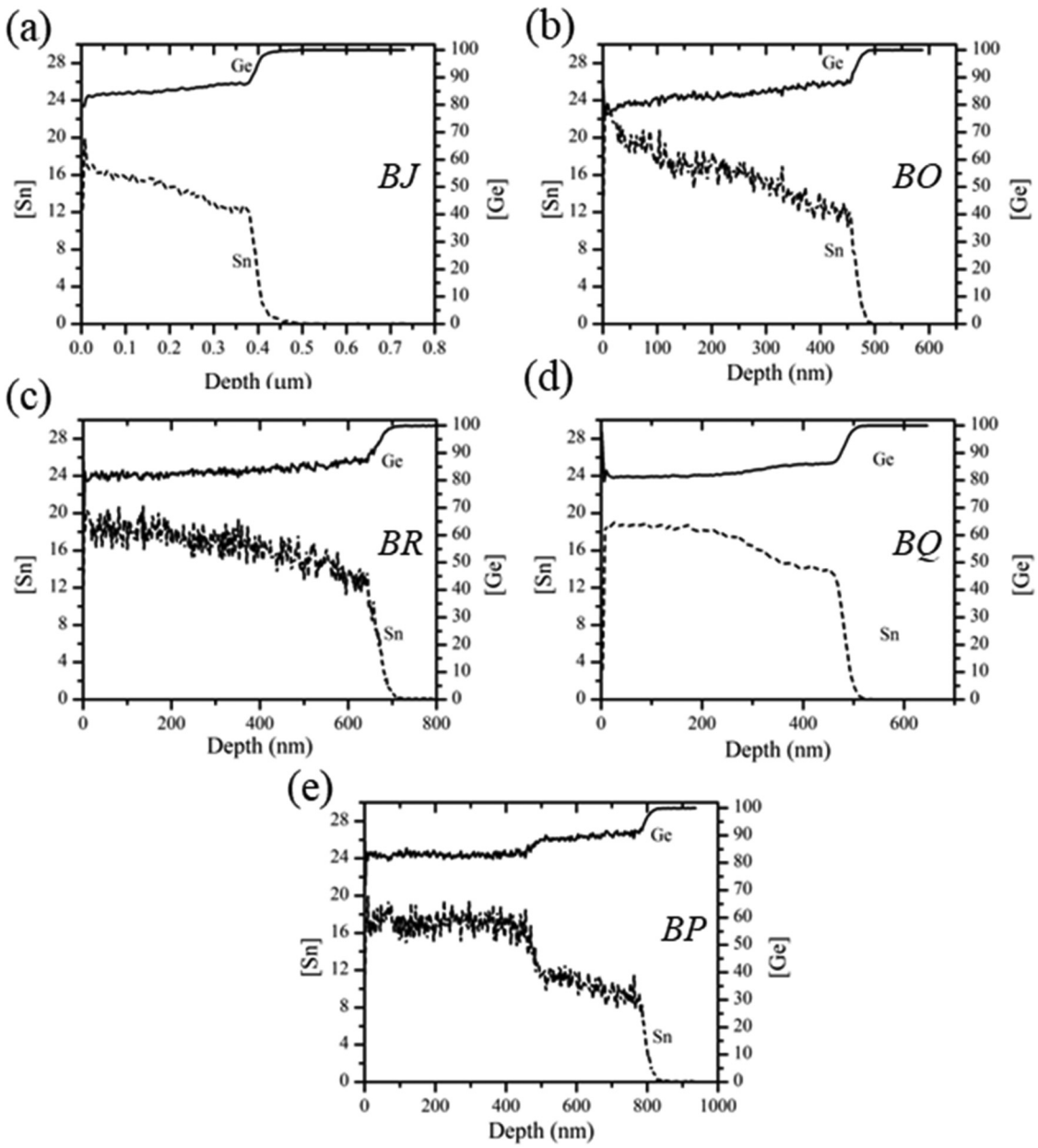

FIG. 9. SIMS profiles of the GeSn films using a [(a)–(d)] single-step and a [(e)] two-step growth process.

parameters for the strained and relaxed layers, respectively. $a_{GeSn}^{relaxed}$ was calculated from the reciprocal values Q_{220} and Q_{004} and a linearly interpolated Poisson ratio value between Ge and Sn. The calculated Sn concentration from the RSM data is consistent with that extracted values from the SIMS profiles. The single-step process samples (*BJ*, *BO*, *BQ*, and *BR*), shown in Figs. 10(a)–10(d) exhibit a shoulder above the (224) GeSn peak, corresponding to the graded GeSn region as observed in the SIMS data [see Figs. 9(a)–9(d)]. The two-step growth process in sample *BP* exhibits two well-resolved (224) GeSn peaks as shown in Fig. 10(e), confirming a bilayer structure formed by the growth interruption.

3. Surface roughness and defect density

The GeSn surface roughness and defect density were measured by AFM. The GeSn surfaces exhibit a cross-hatch pattern

indicating that the film has relaxed by the formation of misfit dislocations as shown in Fig. 11. We observe that the R_a and R_q values increase with GeSn layer thickness and Sn composition as shown in Table I. The threading dislocation density (TDD) varied from $3.5–9.9 \times 10^7/cm^2$ with no overall trend with growth process for the resulting films. We do observe that the TDD decreases with increasing GeSn film thickness with all other growth parameters fixed as seen in Figs. 11(a) and 11(b) and results in Table I.

4. Photoluminescence

Five GeSn films were studied by room-temperature and low-temperature PL to correlate the peak emission with Sn incorporation. Figure 12 depicts the room-temperature PL spectra of four samples *AF*, *AG*, *AH*, and *AN* with Sn compositions of 2.0, 3.0, 4.2, and 7.24%, and film thicknesses of 240, 164, 109, and 130 nm, respectively. The PL spectra exhibit an asymmetric PL lineshape

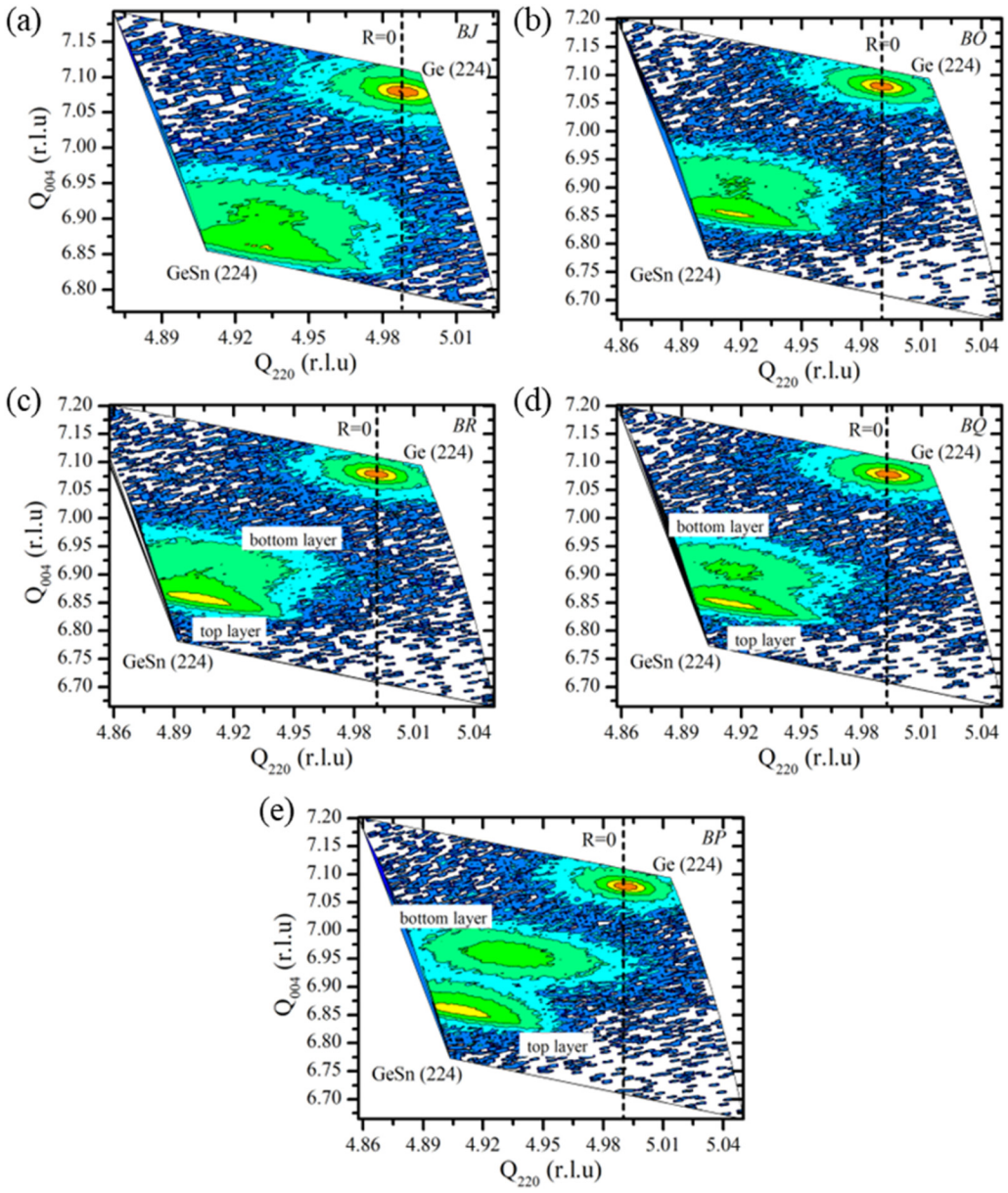

FIG. 10. (224) GeSn and (224) Ge diffraction spots for samples (a) *BJ*, (b) *BO*, (c) *BR*, (d) *BQ*, and (e) *BP*, measured by RSM. The center of the diffraction spot corresponds to the Ge buffer layer. The shoulders above the GeSn diffraction spot are due to strain relaxation and spontaneous composition grading in the GeSn film.

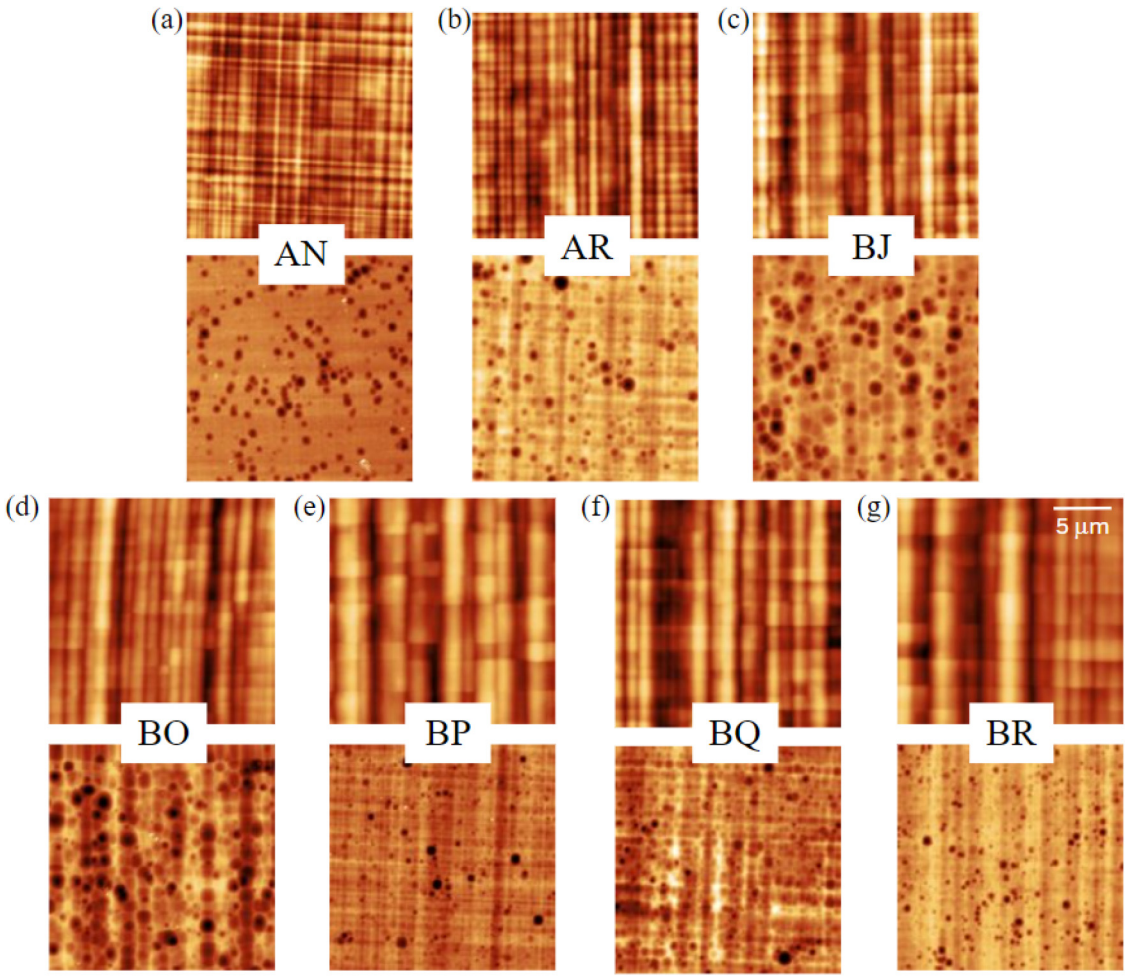

FIG. 11. 20 × 20 μm^2 AFM scans of (a)–(g) As-deposited roughness (top) and corresponding TDD post decorative etch (bottom).

where the maximum peak at 1550 nm for *AF*, *AG*, and *AH* corresponds to the emission of the underlying Ge buffer layer. Sample *AN* does not exhibit luminescence from the Ge buffer layer, possibly due to the increase in absorption coefficient in the GeSn film for higher Sn content, where an indirect to direct bandgap transition may have occurred (between 6% and 12% Sn).[8–10] The second peak on the longer wavelength shoulder of the Ge peak is attributed to the GeSn luminescence. The redshift of the GeSn peak from *AF* to *AN* suggests an increase in Sn incorporation into the Ge lattice. The drop in PL intensity with increasing Sn may not be related to Sn but to the decrease in film thickness where the film quality is expected to be lower, i.e., higher defect density, as it gets closer to the GeSn/Ge heterointerface.

Further, we compared the optical quality of GeSn as a function of thickness and compressive strain. The deposition time for *AR* is two times that of *AN* providing about twice the GeSn layer thickness. As the GeSn thickness increases, the film relaxes from 6% to 64%, facilitating the incorporation of Sn as shown in Table I. The effect of strain relaxation can be observed by the large PL emission redshift between AN and AR, as shown in Fig. 13.

The increase in PL intensity at 20 K for *AR* with respect to *AN* could be related to the reduced density of threading dislocations which act as nonradiative recombination centers. The optical characteristics of GeSn films grown at different $SnCl_4$ flow rates, Sn content, deposition time, GeH_4 flow rates, and number of growth steps was studied by comparing the PL of samples at a temperature of 20 K as shown in Fig. 14. Sample *BO* was grown with ~30% increase in the $SnCl_4$ molar flow rate compared to *BJ* resulting in an increase in thickness, degree of relaxation, and %Sn as shown in Table I. Thus, sample *BO* exhibits a PL emission at 3100 nm, a 200-nm redshift from sample *BJ*, as shown in Fig. 14. Sample *BQ* was grown with a 30% increase in the volumetric GeH_4 flow rate compared to sample *BO*. As shown in Table I, the Sn composition for both *BO* and *BQ* reveal a bilayer structure with similar

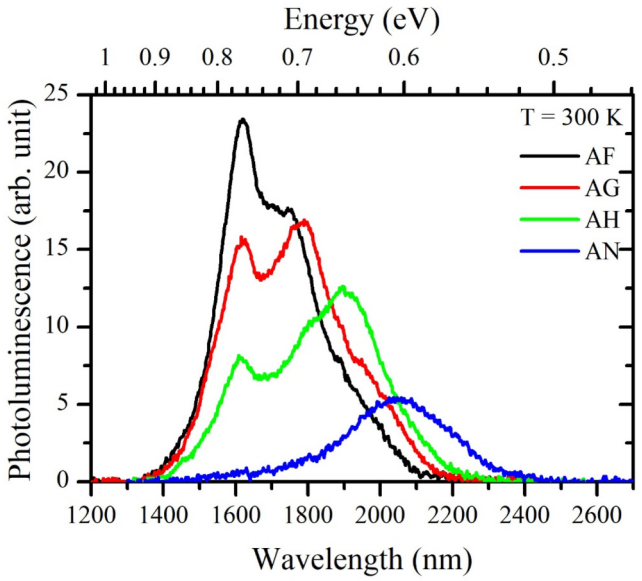

FIG. 12. RT PL band edge emission and intensity by %Sn.

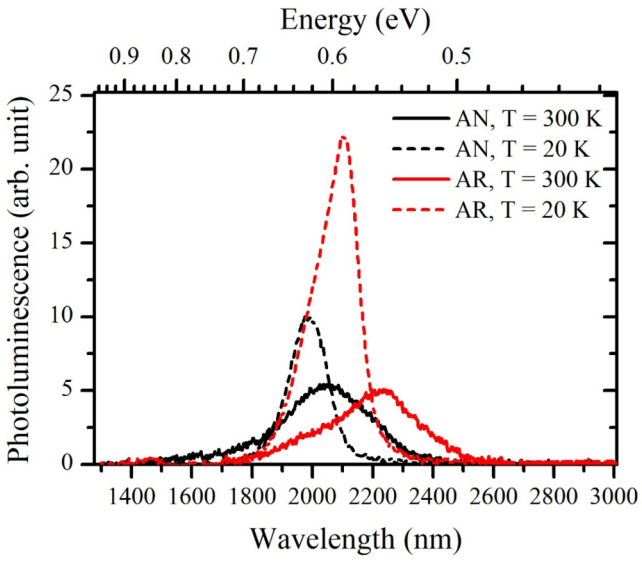

FIG. 13. PL peak location and intensity for *AN* and *AR*.

compositions of 14% Sn in the first layer and 17% Sn in the second layer. The layer thickness and degree of relaxation are also similar. The PL intensity is lower for *BQ*, which might be related to the higher TDD as shown in Table I. But the emission wavelength is showing a 150-nm redshift using the higher GeH_4 flow rate which we are unable to explain based on the nearly identical Sn

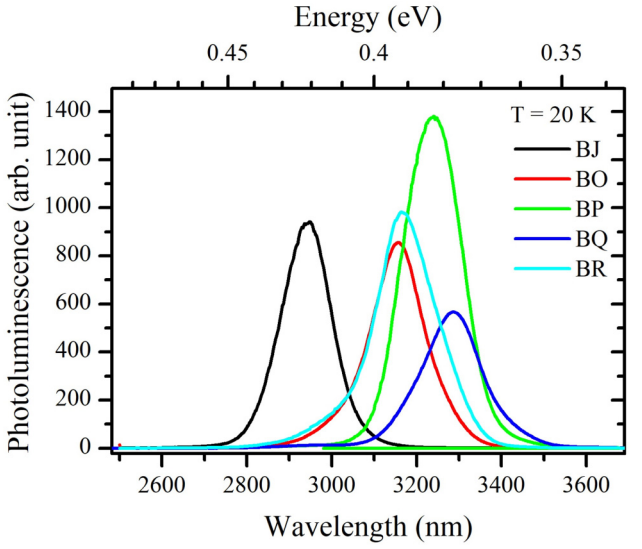

FIG. 14. 20 K PL for GeSn samples *BJ*, *BO*, *BP*, *BQ*, and *BR*.

composition and degree of relaxation measured for *BO* to *BQ*. Sample *BR* was grown with a 30% increase in deposition time compared to *BO*. Hence, for *BR*, we see a higher Sn composition and degree of relaxation as shown in Table I and consequentially a slight redshift in the PL emission and increased PL intensity as shown in Fig. 14. It is worth noting that sample *BP*, grown by the two-step process, exhibits the highest PL intensity. We speculate that the material quality in a two-step growth process is higher than the single-step growth process.

IV. SUMMARY AND CONCLUSIONS

GeSn films with Sn compositions ranging from 2% to 20% have been deposited onto a Ge buffer layer grown on 200 mm silicon substrates using the ASM Epsilon 2000 CVD reactor platform. Sn segregation has been studied as a function of growth parameters including hydrogen carrier gas, $SnCl_4$ molar flow rate, $GeH_4/SnCL_4$ molar flow ratio, and deposition temperature, and fully specular GeSn surfaces have been demonstrated across an entire 200-mm wafer. During the material optimization step, we found that (1) there is some temperature dependence on the GeSn growth rate over a broad temperature range, (2) thickness uniformity tuning using center to edge temperature offsets of 10 °C was ineffectual compared to adjusting the multiport flow injectors, suggesting that growth takes place in the mass transport limited growth regime, and (3) Sn incorporation in GeSn is inversely related to deposition temperature consistent with early studies on CVD-grown GeSn films. Room-temperature PL studies suggest the transition from indirect to direct bandgap behavior occurs at ~7% Sn consistent with previous reports Due to spontaneous strain relaxation and associated increase in %Sn at the growing interface, 22% Sn was achieved near the surface of a GeSn layer using a single-step growth process. The two-step growth process resulted in

two layers consisting of a fully relaxed GeSn layer followed by a higher quality GeSn layer with increased Sn content as evident by the high PL intensity and mid-wave infrared band edge emission of 3.2 μm at 20 K. A more detailed study is necessary to evaluate the GeSn film microstructure in terms of local Sn segregation and point defect formation to further understand the effects of these on the crystalline quality and optoelectronic properties of GeSn films.

ACKNOWLEDGMENTS

This work was supported in part by the Office of Naval Research (Grant Nos. N00014-23-1-2008 and N00014-23-1-2873) and by the Air Force Office of Scientific Research (Grant No. FA9550-22-1-0493).

AUTHOR DECLARATIONS

Conflict of Interest

The authors have no conflicts to disclose.

Author Contributions

Nicholas Rosson: Formal analysis (equal); Methodology (lead); Writing – review & editing (equal). **Sudip Acharya:** Writing – review & editing (equal). **Alec M. Fischer:** Formal analysis (supporting); Writing – review & editing (equal). **Bria Collier:** Data curation (equal). **Abdulla Ali:** Data curation (equal). **Ali Torabi:** Writing – review & editing (supporting). **Wei Du:** Writing – review & editing (equal). **Shui-Qing Yu:** Conceptualization (equal); Funding acquisition (lead); Investigation (supporting); Project administration (lead); Writing – review & editing (supporting). **Robin C. Scott:** Formal analysis (equal); Investigation (equal); Writing – original draft (equal).

DATA AVAILABILITY

The data that support the findings of this study are available from the corresponding author upon reasonable request.

REFERENCES

[1]Y.-H. Ko, K.-J. Kim, and Won Seok Han, Opt. Mater. Express **11**, 943 (2021).
[2]See https://en.wikipedia.org/wiki/Lattice_constant.
[3]V. K. Yang, M. Groenert, C. W. Leitz, A. J. Pitera, M. T. Currie, and E. A. Fitzgerald, J. Appl. Phys. **93**, 3859 (2003).
[4]D. Andrijasevic, M. Austerer, A. M. Andrews, P. Klang, W. Schrenk, and G. Strasser, Appl. Phys. Lett. **92**, 051117 (2008).
[5]A. Tanaka, Toxicol. Appl. Pharm. **198**, 405 (2004).
[6]J. Kouvetakis and A. V. G. Chizmeshya, J. Mat. Chem. **17**, 1649 (2007).
[7]A. H. Atabaki *et al.*, Nature **556**, 349 (2018).
[8]S. A. Ghetmiri *et al.*, Appl. Phys. Lett. **105**, 151109 (2014).
[9]W. Du *et al.*, Appl. Phys. Lett. **105**, 051104 (2014).
[10]J. Rudie, "XPS and IPE determination of band offsets of germanium based materials," Ph.D. dissertation (University of Arkansas, 2022).
[11]R. Cheng, Z. Chen, S. C. Yuan, M. Takenaka, S. Takagi, G. Q. Han, and R. Zhang, J. Semicond. **42**, 023101 (2021).
[12]J. Margetis *et al.*, ACS Photonics **5**, 827 (2017).
[13]D. Stange *et al.*, ACS Photonics **3**, 1279 (2016).
[14]C.-T. Tai, P.-Y. Chiu, C.-Y. Liu, H.-S. Kao, C. T. Harris, T.-M. Lu, C.-T. Hsieh, S.-W. Chang, and J.-Y. Li, Adv. Mater. **33**, 2007862 (2021).
[15]A. Harwit, P. R. Pukite, J. Angilello, and S. S. Iyer, Thin Solid Films **184**, 395 (1990).
[16]S. Kim, N. Bhargava, J. Gupta, M. Coppinger, and J. Kolodzey, Opt. Express **22**, 11029 (2014).
[17]A. Mosleh, S. A. Ghetmiri, B. R. Conley, M. Hawkridge, M. Benamara, A. Nazzal, J. Tolle, S.-Q. Yu, and H. A. Naseem, J. Electron. Mater. **43**, 938 (2014).
[18]J. Tolle, A. V. G. Chizmeshya, Y.-Y. Fang, J. Kouvetakis, V. R. D'Costa, C.-W. Hu, J. Menéndez, and I. S. T. Tsong, Appl. Phys. Lett. **89**, 231924 (2006).
[19]S. Q. Lim, L. Q. Huston, L. A. Smillie, G. J. Grzybowski, X. Huang, J. S. Williams, and B. B. Claflin, J. Appl. Phys. **133**, 235302 (2023).
[20]N. von den Driesch *et al.*, Chem. Mater **27**, 4693 (2015).
[21]S. Wirths, D. Buca, G. Mussler, A. T. Tiedemann, B. Holländer, P. Bernardy, T. Stoica, D. Grützmacher, and S. Mantl, ECS J. Solid State Sci. Technol. **2**, N99 (2013).
[22]H. Tran *et al.*, ACS Photonics **6**, 2807 (2019).
[23]H. Ye and J. Yu, Sci. Technol. Adv. Mater. **15**, 024601 (2014).
[24]Z. Kong *et al.*, Nanomaterials **12**, 981 (2022).
[25]W. C. Dash, J. Appl. Phys. **29**, 228 (1958).
[26]Y. Miao *et al.*, Nanomaterials **11**, 2556 (2021).
[27]J. Margetis, "RPCVD growth of Si-Ge-Sn alloys for optoelectronics applications," Ph.D. dissertation (Arizona State University, 2018).
[28]Y.-H. Kil, S.-H. Yuk, H.-S. Jang, S.-G. Lee, C.-J. Choi, and K.-H. Shim, Electron. Mater. Lett. **14**, 207 (2018).
[29]J. Margetis *et al.*, ECS Trans. **64**, 711 (2014).
[30]P. C. Grant *et al.*, Opt. Mater. Express **9**, 3277 (2019).
[31]Process Training Manual—Epsilon one Model—E2 Epsilon (ASM, 1992).
[32]F. Gencarelli *et al.*, ECS J. Solid State Sci. Technol. **2**, 134 (2013).
[33]W. Dou *et al.*, Sci. Rep. **8**, 5640 (2018).
[34]S. Assali, J. Nicolas, S. Mukherjee, A. Dijkstra, and O. Moutanabbir, Appl. Phys. Lett. **112**, 251903 (2018).